ELSEVIER

Chemical Engineering Journal 138 (2008) 523–537

Chemical Engineering Journal

www.elsevier.com/locate/cej

On the estimate of mixing length in interdigital micromixers

Stefano Cerbelli, Massimiliano Giona *

Dipartimento di Ingegneria Chimica, Facoltà di Ingegneria, Università di Roma "La Sapienza", via Eudossiana 18, 00184 Roma, Italy

Received 13 April 2007; received in revised form 12 June 2007; accepted 6 July 2007

Abstract

The multilamination process that characterizes interdigital micromixers is an efficient and technologically feasible method for maximizing and controlling mass and/or heat transfer between two or more segregated fluid streams. We analyze the dynamics of mixing that takes place in the mixing channel downstream the interdigital apparatus. Specifically, we investigate, for different flow profiles, how the channel length necessary to achieve a prescribed level of mixedness depends on the degree of lamination (number and thickness of lamellae) of the feed stream. As a case study, we consider plug, shear and Poiseuille flow, and compare steady-state profiles resulting from the numerical simulation of the full advection–diffusion problem with the analytical solution stemming from the one-dimensional Sturm–Liouville eigenvalue problem along the spanwise coordinate, obtained neglecting streamwise diffusion. We find that (i) the mixing length can be significantly affected by the flow profile, especially at high degree of lamination of the feed stream, and (ii) in general, no obvious scaling between mixing length and lamellar thickness can be assumed. A rigorous way to approach the design of these micromixers is proposed.

Keywords: Fluid mixing; Interdigital micromixers; Laminar flows; Homogenization; Lamination

1. Background and motivation

Interdigital micromixers provide a novel technology that allows to accomplish a nearly complete homogenization of two or more segregated fluid streams within extremely short contact times (e.g. up to order of milliseconds in the case of liquids, see [1] and therein cited references). Other uses of these devices include microreactions as microextraction [2], as well as liquid–liquid dispersion [3]. The simplest case of "T-junction" channel is also used for sensing and separating analytes [4,5], measuring diffusivities and determining kinetic rate constants [6].

The core of the equipment is constituted by a comb-like arrangement of microchannels that split the streams entering the system and rearrange them into a multilaminated structure where alternating *lamellae* of the two fluids are forced to flow alongside. The typical width of one of such lamellae is of the order of tens of micron. The spatially periodic structure of the process stream is then squeezed into a smaller channel, referred to as mixing channel, where the desired degree of mixing is reached.

Typically, the micromixers are identified by the type of geometry connecting the multilamination apparatus and the mixing channel. Frequently used configurations are the rectangular, slit-shaped, triangular, and the super-focus mixer [7,8]. Fig. 1 shows a schematic representation of the rectangular micromixer.

Apart from specific cases, such as that of relatively high Reynolds number flow (e.g. order $Re = 10^3$) in the slit-shaped micromixer, little mixing occurs in the portion of the apparatus connecting the multilamination device and the mixing channel. As a result, the flow stream at the entrance of the mixing channel can be thought of as an ordered array of alternating lamellae [8], each characterized by a constant concentration of one of the species that are to be mixed.

Beside lowering substantially the mixing time associated with advecting–diffusing species, the number and width of the lamellae can also have a strong influence on the performance of the device in the case where the two species are chemically reactive. As an example, numerical simulations suggest that the degree of lamination of reactants fed to a microreaction channel can impact substantially on the yield and product distribution of parallel-competitive and parallel-consecutive reactions [9].

* Corresponding author. Tel.: +39 06 44585892; fax: +39 06 44585451.
E-mail address: max@giona.ing.uniroma1.it (M. Giona).

1385-8947/$ – see front matter © 2007 Elsevier B.V. All rights reserved.
doi:10.1016/j.cej.2007.07.067

Nomenclature

$\mathrm{Ai}(z)$	Airy function of first kind
$\mathrm{Bi}(z)$	Airy function of second kind
C_h	generalized Fourier coefficients defined by Eq. (15)
$\mathcal{D}$	diffusivity
L	channel length
n_s	number of lamellae of the inlet concentration profile
Pe	Peclet number, $Pe = \delta^2 U/\mathcal{D}L$
s	lamellar width
U	characteristic mean velocity
$v_x(y)$	dimensionless axial velocity
x	dimensionless axial coordinate
y	dimensionless vertical coordinate
Y_h	eigenfunctions of the Sturm–Liouville problem

Greek letters

α	reciprocal of the aspect ratio, $\alpha = \delta/L$
δ	channel width
λ_h	eigenvalue of the Sturm–Liouville operator
μ	degree of mixedness
ξ	Pe-scaled axial coordinate $\xi = x/Pe$
$\sigma(x)$	variance of the concentration profile at x
σ_v	variance ratio defined by Eq. (6)
ϕ	dimensionless solute concentration
$\phi_i(y)$	inlet concentration profile
$\phi_i^{(n_s)}$	inlet lamellar profile defined by Eq. (4)

When designing micromixers, an important piece of information is an *a priori* estimate of the mixing performance associated with a given lamellar thickness, say s, of the feed stream. Specifically, one would like to estimate the length, L, of the channel that ensures a prescribed level of mixedness at the system outlet section.

An analytical estimate of the mixing length is usually obtained by invoking simplifying assumptions in the solution of the steady-state advection–diffusion problem, namely: (i) flat velocity profile (plug flow), (ii) high value of the channel aspect ratio (semi-infinite channel), and (iii) substitution of the zero diffusive flux condition at the channel walls with periodic boundary conditions in the spanwise direction[1].

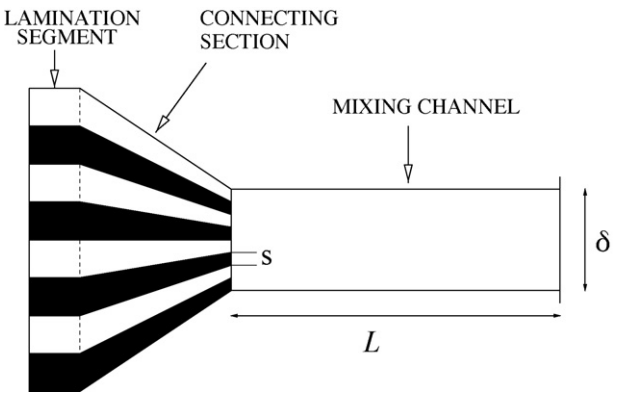

Fig. 1. Schematic diagram of the rectangular interdigital micromixer.

Under these assumptions, the advection–diffusion boundary value problem is recast into a simpler partial differential problem that is formally identical to a standard one-dimensional unsteady diffusion problem, where the relationship between time, say T, and length of the channel is given by the ratio between L and the convective mean velocity, say U, i.e. $T = L/U$. By using these approximations, a scaling relationship $T \sim s^2$ or, equivalently, $L \sim s^2$, is obtained (see, e.g. [2,11]). Furthermore, this scaling relationship results *independent of the level of mixedness* required (a derivation of this result is discussed in detail in Appendix A).

In this article, we challenge this estimate and analyze separately the role of each simplifying assumption. The analysis is carried out by using three prototypical flow profiles, namely plug, shear, and Poiseuille flow, which are frequently encountered in microhydrodynamic applications. Specifically, plug-like velocity profiles are encountered in electroosmotically driven flows [12], while the shear profile, typical of micromotors and microbearings [13], can in principle be obtained by electroosmosis through an asymmetric surface treatment of the channel walls. The Poiseuille profile characterizes pressure-driven microflows.

We compare and contrast results from direct numerical simulations of the full advection–diffusion equation with the solution of the simplified transport equation stemming from the high-aspect ratio approximation, which is equivalent to a one-dimensional unsteady diffusion problem with variable diffusivity along the spanwise coordinate. The analysis of this problem reduces to finding the eigenvalue–eigenfunction spectrum of a Sturm–Liouville second-order problem specified by the flow profile.

The article is organized as follows. Section 2 introduces the physical problem, and its mathematical and computational formulation. Section 3 addresses the Sturm–Liouville approach for high-aspect ratio microchannels, and the spectral (eigenvalue/eigenfunction) structure of the resulting advection–diffusion operator. Specifically, Section 3.3 derives the main results for typical laminar flows in microchannels, and Section 3.4 introduces a quantitative way for the design of interdigital micromixers based on the Sturm–Liouville formulation discussed in Section 3.3. It is shown that the classical scaling law $L \sim s^2$ (relating the channel length to the lamellar width of the feed stream) it is far from being verified for generic laminar flows. The approach proposed in Section 3.4 provides a simple design strategy for interdigital micromixers. In Appendix

[1] The simplifying assumptions of flat velocity profile and semi-infinite channel (which allow to neglect axial diffusion) are also used to construct one-dimensional models of mixing for predicting the mixing length associated with more complex geometries, such as, e.g. the split-and-recombine mixer [10]. In this context, the effort directed towards the construction of simplified analytical models of the (possibly chaotic) three-dimensional mixing process is motivated by the unavoidable presence of spurious diffusion, which can overshadow the results of numerical simulations when complex flows are dealt with.

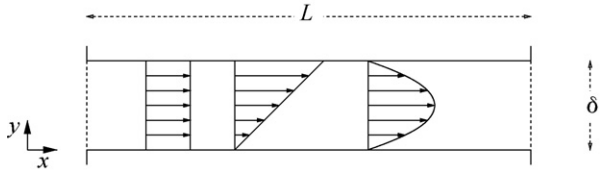

Fig. 2. Sketch of the system geometry.

A added at the end of the article, a rigorous derivation of the ($L \sim s^2$)-scaling is reported, which highlights the role of the simplifying assumptions starting from which this expression holds true.

2. Statement of the problem and numerical solution

2.1. Physical system

We are concerned with the steady-state mixing behavior of a diffusing scalar entering a steady inflow–outflow two-dimensional channel for which the velocity field is one-dimensional (parallel flow). Let $\hat{\phi}(\hat{x}, \hat{y})$ denote the scalar field, and let $\Omega = \{(\hat{x}, \hat{y}) | \hat{x} \in [0, L], \hat{y} \in [0, \delta]\}$ be the channel domain (see Fig. 2). The dimensional formulation of the advection–diffusion equation reads:

$$\hat{v}_{\hat{x}}(\hat{y}) \frac{\partial \hat{\phi}}{\partial \hat{x}} = \mathcal{D} \left(\frac{\partial^2 \hat{\phi}}{\partial \hat{x}^2} + \frac{\partial^2 \hat{\phi}}{\partial \hat{y}^2} \right), \tag{1}$$

where $\hat{v}_{\hat{x}}(\hat{y})$ is the velocity profile and $\mathcal{D}$ is the bare molecular diffusivity. Here $\hat{\phi}$ can be thought of as representing the difference, $\hat{\phi} = c_A - c_B$ of the concentrations c_A, c_B of two chemical species A and B possessing the same bare molecular diffusivity $\mathcal{D}$. In this context, it is also worth noting that, in the case of stoichiometric feeding (i.e. when $\int_0^1 \hat{v}_{\hat{x}}(\hat{y}) \hat{\phi}(0, \hat{y}) \, d\hat{y} = 0$), the solution of Eq. (1) also provides complete information on the evolution of a mixing-controlled reaction A + B → products [14–16].

In general, the profile $\hat{v}_{\hat{x}}(\hat{y})$ can be regarded as a solution of the Stokes problem in the (possibly contemporary) presence of pressure gradients, electroosmotic body forces, or moving boundaries. In what follows, we consider three prototypical cases, namely plug, shear and the (pressure-driven) Poiseuille flow, i.e. given by $\hat{v}_{\hat{x}}(\hat{y}) = U$, $\hat{v}_{\hat{x}}(\hat{y}) = 2U\hat{y}/\delta$, and $\hat{v}_{\hat{x}}(\hat{y}) = 6U(1 - \hat{y}/\delta)\, \hat{y}/\delta$, respectively, U being the average velocity over the channel cross-section.

2.2. Dimensionless formulation and boundary conditions

Let us first consider a dimensionless formulation of the problem. By setting $\hat{x} = L\,x$, $\hat{y} = \delta\,y$, $\alpha = \delta/L$, $U = (1/\delta) \int_0^\delta \hat{v}_{\hat{x}}(\hat{y}) \, d\hat{y}$ as a reference velocity (i.e. U is the average velocity over the channel cross-section), $v_x(y) = \hat{v}_{\hat{x}}(\hat{y}/\delta)/U$, $\phi(x, y) = \hat{\phi}(\hat{x}/L, \hat{y}/\delta)/F$, with $F = \max_{\hat{y} \in [0,\delta]} \hat{\phi}(0, \hat{y})$, one obtains the dimensionless equation:

$$v_x(y) \frac{\partial \phi}{\partial x} = \frac{1}{Pe} \left(\alpha^2 \frac{\partial^2 \phi}{\partial x^2} + \frac{\partial^2 \phi}{\partial y^2} \right), \tag{2}$$

where $Pe = \delta^2 U/(\mathcal{D}L)$ is the Peclet number representing the ratio of the characteristic time for diffusion, $\tau_d = \delta^2/\mathcal{D}$, to that of advection, $\tau_a = L/U$, and where the scaled coordinates (x, y) belong to the unit square domain $[0, 1] \times [0, 1]$. The reciprocal $1/\alpha$ of the parameter α is henceforth referred to as the aspect ratio.

At the channel walls (assumed impermeable to the diffusing scalar), a zero diffusive flux condition applies, i.e.:

$$\left. \frac{\partial \phi}{\partial y} \right|_{y=0} = \left. \frac{\partial \phi}{\partial y} \right|_{y=1} = 0. \tag{3}$$

At the entrance section, we consider the profile assigned, i.e. $\phi(0, y) = \phi_i(y)$, where $\phi_i(y)$ is given and depends on the inlet conditions. As the main focus of this article is to assess the homogenization length associated with a lamellar entrance condition, as that generated by an interdigital micromixer, for $\phi_i(y)$ we choose a stepwise function of frequency $s = 1/n_s$:

$$\phi_i^{(n_s)}(y) = \begin{cases} 1 & \text{if } 2h/n_s \le y \le (2h+1)/n_s \\ -1 & \text{if } 2h + 1/n_s \le y \le 2(h+1)/n_s, \end{cases} \tag{4}$$

with $h = 0, 1, 2, \ldots (n_s - 1)/2$, representing an array of n alternating *lamellae* of thickness s, each characterized by a unit concentration of one of the two species A or B (see Fig. 3). As it regards the outlet section, a zero diffusive flux condition referred to as the Danckwerts boundary condition is assumed, i.e.:

$$\left. \frac{\partial \phi}{\partial x} \right|_{x=1} = 0. \tag{5}$$

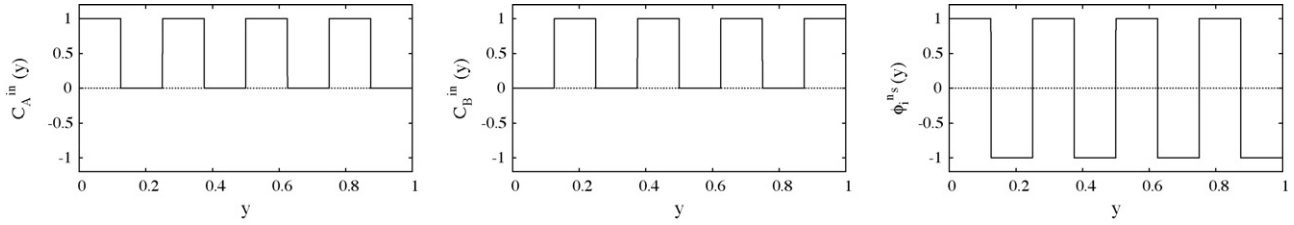

Fig. 3. Inlet profile of the (dimensionless) species concentrations c_A^{in} and c_B^{in} associated with $\phi_i^{(n_s)}(y) = c_A^{in} - c_B^{in}$ for $n_s = 8$.

2.3. Quantitative assessment of mixing efficiency

In what follows, we choose as a measure of mixedness the ratio:

$$\sigma_v(x) = \frac{\sigma(x)}{\sigma(0)}, \tag{6}$$

between the velocity-weighted scalar variance computed at the generic cross-section at x, and inlet sections, respectively, where $\sigma(x)$ is defined as

$$\sigma^2(x) = \int_0^1 v_x(y)\big(\phi(x,\, y) - \overline{\phi}(x)\big)^2 \,\mathrm{d}y, \tag{7}$$

and where $\overline{\phi}(x) = \int_0^1 v_x(y)\phi(x,\, y)\,\mathrm{d}y$ is the cross-sectional average of the concentration at x (note that the total volumetric flow rate across any cross-section is unity in the dimensionless formulation). Borrowing an expression from a classical book [17], the scalar variance defined by Eq. (7) could be defined as a "cup-mixing" variance, i.e. it is equal to the scalar variance that one would measure in a mixture obtained by collecting and quenching the entire flowrate exiting the cross-section at the specified x for a time interval Δt. Therefore, the variance defined by Eq. (7) should be regarded as a generalization of the scalar variance customarily used in closed systems to quantify mixing efficiency, where one takes into account that the material flows at different rate at a generic point of the cross-section, the rate being the local velocity that appears as a weighting factor.

In the limit where $Pe \to \infty$, the scalar variance is conserved through the channel, and therefore $\sigma_v = 1$. In this case, no mixing occurs. On the other hand, when $Pe \to 0$, a perfectly mixed state characterizes the outlet profile, independently of the structure of the velocity profile. For this case it results $\sigma_v(1) = 0$.

However, none of the two limit situations is typical in microflows. In fact, the order of magnitude of the Pe number in practical realizations of microfluidic devices can range in the interval $[10^{-1}, 10^3]$ leading to the conclusion that there is no typical Pe number in microflows [18].

2.4. Numerical solution

The numerical solution of the boundary value problem defined in the previous section was obtained by means of a standard finite-volume relaxation method. Specifically, as it regards the convective term, standard upwind differencing scheme was used.

Values of the Pe parameter between 10^1 and 10^3, and of the aspect ratio $1/\alpha$ between 10 and 50 were considered.

The number of cell volumes, N_c varied from a minimum of order 5×10^4 to a maximum of order 10^6 cells, depending on the number of lamellae characterizing the feed stream, and on the Pe value. For each simulation, the number of cells was chosen as the minimum required to ensure that numerical diffusion could be neglected (i.e. a further mesh refinement would not produce changes on the profile at steady state).

As an example, Fig. 4(a) and (b) shows the outlet concentration profiles at steady state for different levels of discretization for an inlet condition corresponding to eight lamellae for the case of parabolic (Poiseuille) flow at $Pe = 10$ and 10^2, respectively, and a value $\alpha = 10^{-1}$ of the reciprocal aspect ratio. As can be observed, independence of the discretization level is already reached at order 10^5 cells in both cases. The largest number of cells considered, $N_c = 1000 \times 640$, resulted for the case of an inlet condition consisting of $n_s = 32$ lamellae.

Next, let us analyze mixing performance associated with different flow profiles and different values of the aspect ratio $1/\alpha$. Fig. 5 shows the decay of the normalized scalar variance $\sigma_v(x)$ along the axial coordinate for two inlet conditions (consisting of two and eight lamellae) for the Poiseuille and plug flows, corresponding to different values of the aspect ratio $1/\alpha$. From the analysis of variance decay associated with the two inlet profiles, several observations can be made.

First, in the case of two lamellae, neither the flow profile nor the aspect ratio has a strong impact on mixing performance (compare curve A in Fig. 5(a) and (b)—note that the scale of the two panels is different). As it regards the performance of the plug flow (Fig. 5(b)), pushing the degree of lamination, from $n_s = 2$ (curve A) to $n_s = 8$ lamellae (curve B), does not improve mixing

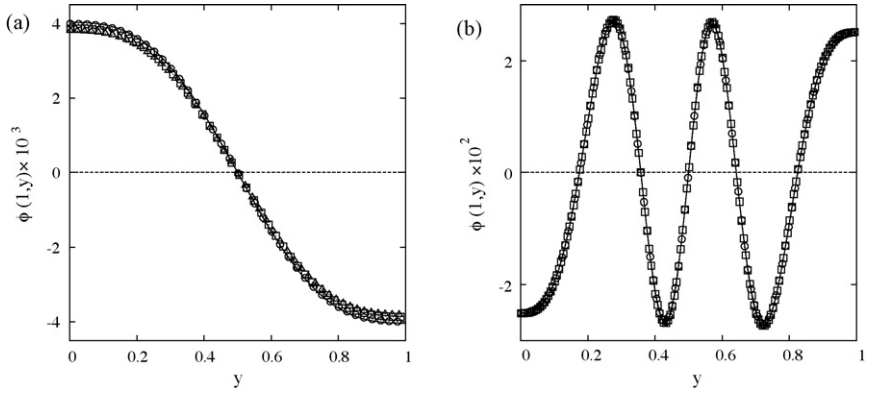

Fig. 4. Outlet profiles for different discretization levels for the Poiseuille flow at $1/\alpha = 10$ and for an inlet condition consisting of eight lamellae. Panel (a) $Pe = 10$. (△) $N_c = 240 \times 240$; (□) $N_c = 320 \times 320$; (◯) $N_c = 640 \times 320$; continuous line: $N_c = 960 \times 320$. Panel (b) $Pe = 10^2$. (□) $N_c = 320 \times 320$; (◯) $N_c = 640 \times 320$; continuous line: $N_c = 960 \times 320$.

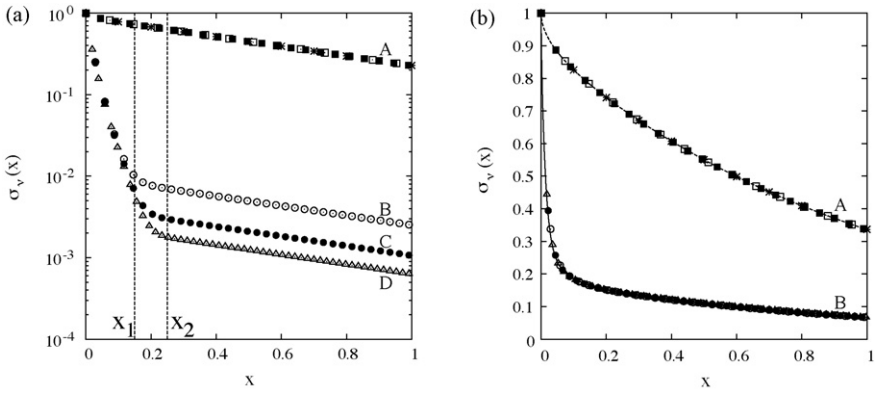

Fig. 5. Axial decay of normalized scalar variance for different degrees of lamination, $n_s = 2,\ 8$ and different values of the aspect ratio $1/\alpha$ at $Pe = 10$. Panel (a) Poiseuille flow. (*) $1/\alpha = 10$, $n_s = 2$; (□) $1/\alpha = 20$, $n_s = 2$; (■) $1/\alpha = 50$, $n_s = 2$.(◯) $1/\alpha = 10$, $n_s = 8$; (◯) $1/\alpha = 20$, $n_s = 8$; (△) $1/\alpha = 50$, $n_s = 8$. Panel (b) plug flow. Symbols are consistent with panel (a).

quality as one would expect from the analytical estimate of the simplified setting discussed in Appendix A.

The situation is rather different when the higher laminated inlet stream ($n_s = 8$) is fed to the parabolic flow profile (curves B–D of Fig. 5(a)). In this case, independence of the solution of the aspect ratio is reached at values of the aspect ratio $1/\alpha \geq 50$ (corresponding to curve C), which implies a difference of three decades between the normalized dimensionless diffusivities ($1/Pe$ and α^2/Pe) associated with the two spatial directions (see Eq. (2)). Also, one can observe that the normalized scalar variance quickly settles onto a strict exponential decay (note that scale of the vertical axis of Fig. 5(a) is logarithmic) with a decay rate that is independent of the channel aspect ratio.

In order to explain the sensitivity to the channel aspect ratio displayed by the eight-lamina feed, let us consider the scalar profiles along the spanwise coordinate at two different positions, $x_1 = 0.15$, and $x_2 = 0.25$ downstream the channel entrance (see Fig. 5(a)). At $x \geq x_2$ the decay rate appears independent of both the channel aspect ratio $1/\alpha$ and the degree of lamination n_s (compare curves A–D of Fig. 5(a)). The analysis of the scalar profile for the different conditions at x_2 shown in Fig. 6(a) and (b) reveals that, although different in absolute values and minor

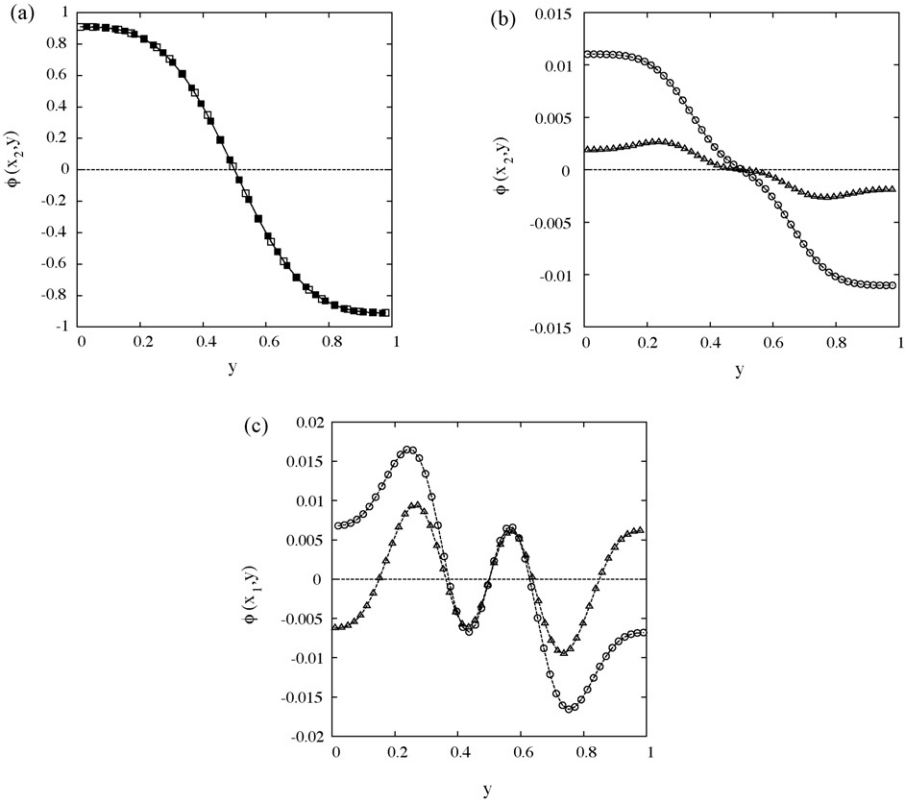

Fig. 6. Scalar concentration profiles along the spanwise coordinate at two different cross-sections, $x_1 = 0.15$ and $x_2 = 0.25$, at $Pe = 10$ for the Poiseuille flow at different values of the aspect ratio $1/\alpha$. Panel (a) $n_s = 2$ at $x = x_2$: (■) $1/\alpha = 10$; (□) $1/\alpha = 50$. Panel (b) $n_s = 8$ at $x = x_2$: (◯) $1/\alpha = 10$; (△) $1/\alpha = 50$. Panel (c) $n_s = 8$ at $x = x_1$: (◯) $1/\alpha = 10$; (△) $1/\alpha = 50$.

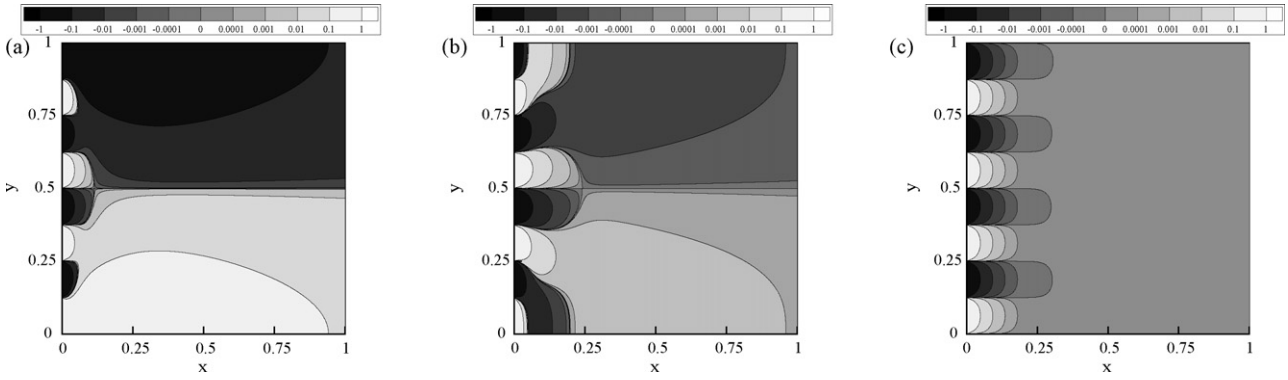

Fig. 7. Contour plot of the scalar profile for the inlet condition $\phi_i^{(n_s)}(y)$, $n_s = 8$, at $Pe = 10$ and $1/\alpha = 50$. Panel (a) plug flow. Panel (b) Poiseuille flow. Panel (c) plug flow with periodic boundary conditions in the spanwise coordinate y. The contour levels are chosen in a logarithmic scale as $-1, -10^{-1}, -10^{-2}, -10^{-3}, -10^{-4}, 0, 10^{-4}, 10^{-3}, 10^{-2}, 10^{-1}$ and 1.

qualitative details, all of the profiles are essentially composed of two lamellae,[2] regardless of α and n_s. Therefore, these data suggest that the *rate* of scalar variance decay at a given position along the streamwise coordinate is essentially related to the number of surviving lamellae at the assigned cross-section. This idea is confirmed by the analysis of the scalar profile associated with the eight-lamina feed (see Fig. 6(c)), taken at a cross-section $x_1 = 0.15$ where the rate of decay is much higher than the "asymptotic" value (compare with the variance decay plot of Fig. 5(a)). The profile associated with a high-aspect ratio, $1/\alpha = 50$ is composed by six lamellae (symbols (Δ) in Fig. 6(c)), whereas that associated with a value $1/\alpha = 10$ (symbols ($\bigcirc$) in the same panel) is composed by four lamellae and is characterized by a slower decay rate. In this case, the presence of a lower streamwise diffusion associated with a high-aspect ratio, $1/\alpha = 50$ is such to sustain a higher number of lamellae with respect to the case $1/\alpha = 10$. On the other hand, in the case of the two-lamina feed ($n_s = 2$) the number of lamellae has reached its minimum already at the entrance section, and therefore the effect of axial diffusion is immaterial under this standpoint.

In the next section, we show that the observations about the decay rate can be put in a simple and rigorous framework by considering the Sturm–Liouville formulation of the advection–diffusion problem. In point of fact, the rate of axial decay of the normalized variance is directly related to eigenvalue associated with the slowest decaying eigenmode of the Sturm–Liouville formulation of the problem.

Before closing this section, we analyze next the influence of the boundary conditions at the channel walls. For both the plug and Poiseuille flows, the role played by the zero diffusive flux at the channel walls appears evident from the analysis of the contour plot of the steady-state scalar field. Fig. 7 shows the contour level structure for plug (Fig. 7(a)) and Poiseuille (Fig. 7(b)) flow at $Pe = 10$ and $1/\alpha = 50$.

The data show the significant role played by the zero-flux boundary conditions in determining the spatial structure of the steady scalar field. Specifically, the contour level lines are "attracted" towards the channel walls in that they must verify the orthogonality condition at these boundaries (i.e. the scalar gradient $\nabla\phi$, that is orthogonal to the contour level curve, must be parallel to the channel walls). It is worth noting that, even in the case of the plug flow, this structure is altogether different from that associated with the solution of the idealized situation of periodic boundary conditions in the spanwise coordinate [2,11], which is depicted in Fig. 7(c) for the same choice of parameters $n_s = 8$, $Pe = 10$, $1/\alpha = 50$.

By the comparison between plug and Poiseuille flows (see Fig. 5(a) and (b)), one observes that mixing performance in the parabolic flow profile for the $n_s = 8$ feed stream is improved by two orders of magnitude with respect to the corresponding case of the plug flow.

In order to understand what is the ultimate reason of the different performance associated with the two velocity profiles, let us analyze the scalar profiles downstream the entrance section. Fig. 8 shows the scalar profile at one tenth ($\bar{x} = 0.1$) of the mixer length for plug and Poiseuille flow for the same parameters of Fig. 7(a) and (b). In the case of plug flow, all of the initial lamellar structure has been destroyed, and the scalar structure consists of essentially two lamellae, whereas in the presence of parabolic flow six lamellae can be still identified. Also, note that even though the maximum of ϕ in Poiseuille flow is an order of magnitude lower than in plug flow, the average magnitude of the scalar gradient normalized with respect to maximum of the scalar profile is higher than the corresponding quantity in the case of plug flow (not shown for brevity). Thus, the reason for the different performance of the two flows can be given by the same qualitative explanation developed above when discussing the dependence of mixing performance on the aspect ratio, i.e. the best performing flow is that capable of maintaining the highest normalized gradients (essentially related to the number of surviving lamellae) in that to higher gradients correspond higher mixing rates. In this respect, the conditions that maximize mixing efficiency in open systems operating at steady state are consistent with those that yield the highest mixing rate in closed advecting–diffusing flows [15,19,20].

[2] In this context, the number of lamellae can be defined as the number of zeros of the spanwise scalar profile augmented by one.

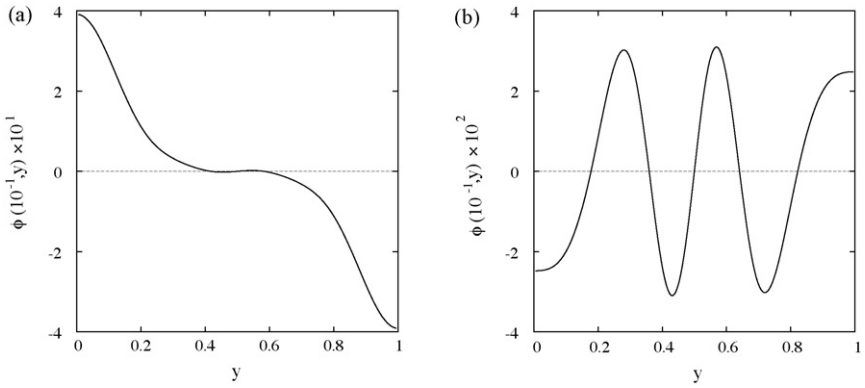

Fig. 8. Scalar profiles $\phi(\overline{x}, y)$ at $\overline{x} = 1/10$ associated with the same set of parameters as those referred in Fig. 7(a) and (b), i.e. $n_s = 8$, $Pe = 10$, $1/\alpha = 50$. Panel (a) plug flow and panel (b) Poiseuille flow. Note that the scale of concentration is different in the two cases.

In the next section, we show that the peculiar behavior of the parabolic flow profile can be interpreted in the framework of the eigenvalue–eigenfunction spectrum associated with the advection–diffusion problem in the limit of vanishing reciprocal aspect ratio, $\alpha \to 0$.

3. High-aspect-ratio channels: Sturm–Liouville solution

Let us then discuss the limiting behavior of Eq. (2) in the case where $\alpha \ll 1$, i.e. when the term $\alpha^2 \partial^2\phi/\partial x^2$ can be neglected, thus leading to the equation:

$$v_x(y)\frac{\partial \phi}{\partial x} = \frac{1}{Pe}\frac{\partial^2 \phi}{\partial y^2}. \tag{8}$$

In this case, it is no longer necessary to specify the outlet boundary condition, namely $\partial\phi/\partial x|_{x=1} = 0$.

The boundary value problem expressed by Eq. (8) and the aforementioned boundary conditions can be approached by separation of variables. By setting $\xi = x/Pe$, $\Phi(\xi, y) = \phi(x/Pe, y)$, Eq. (8) transforms into

$$v_x(y)\frac{\partial \Phi}{\partial \xi} = \frac{\partial^2 \Phi}{\partial y^2}. \tag{9}$$

Upon introducing separation of variables, $\Phi(\xi, y) = X(\xi)\,Y(y)$, Eq. (9) transforms into a Sturm–Liouville eigenvalue problem for the y-dependent function:

$$Y''(y) + \lambda v_x(y) Y(y) = 0, \tag{10}$$

where $Y'(y) = \mathrm{d}Y(y)/\mathrm{d}y$, equipped with the boundary conditions:

$$Y'(0) = Y'(1) = 0, \tag{11}$$

while the corresponding $X(\xi)$ functions satisfy the equation $\mathrm{d}X(\xi)/\mathrm{d}\xi + \lambda X(\xi) = 0$. The eigenvalue problem expressed by Eqs. (10) and (11) admits a countably infinite sequence of real non-negative increasing eigenvalues λ_h, $\lambda_h < \lambda_{h+1}$, $h = 0, 1, \ldots$ (with multiplicity 1), and $\lambda_0 = 0$. The associated eigenfunctions, $Y_h(y)$, constitute a basis for the space of square summable functions $L^2([0, 1])$ defined in $[0, 1]$, possessing vanishing derivative at the interval boundaries. The eigenfunctions $Y_h(y)$s are orthogonal with respect to the weighting function $v_x(y)$, i.e.:

$$\int_0^1 v_x(y)\, Y_k(y)\, Y_h(y)\, \mathrm{d}y = 0, \quad h \neq k. \tag{12}$$

The solution $\Phi(\xi, y)$ is thus given by the series expansion:

$$\Phi(\xi, y) = \sum_{h=0}^{\infty} C_h\, \mathrm{e}^{-\lambda_h \xi} Y_h(y), \tag{13}$$

and, correspondingly, $\phi(x, y)$ is given by

$$\phi(x, y) = \sum_{h=0}^{\infty} C_h\, \exp(-\lambda_h x/Pe) Y_h(y), \tag{14}$$

Eq. (14) shows the explicit dependence on the Pe number of the solution of the advection–diffusion equation.

The coefficients C_h are uniquely identified by the inlet condition, and read as

$$C_h = \frac{\int_0^1 v_x(y)\phi_i^{(n_s)}(y) Y_h(y)\, \mathrm{d}y}{\int_0^1 v_x(y) Y_h^2(y)\, \mathrm{d}y}, \tag{15}$$

which stems from Eq. (13) and from the orthogonality condition (Eq. (12)). As it regards the scalar variance $\sigma^2(\xi) = \sigma^2(x/Pe) = \int_0^1 v_x(y)(\phi - \overline{\phi})^2\, \mathrm{d}y$, the orthogonality of the eigenfunctions implies that

$$\sigma^2(\xi) = \sum_{h=1}^{\infty} C_h^2\, \exp(-2\xi\lambda_h) D_h,$$

$$D_h = \int_0^1 v_x(y) Y_h^2(y)\, \mathrm{d}y, \tag{16}$$

where D_h are normalization coefficients that do not depend on the inlet condition. This equation shows that the ξ-dependence of the squared scalar variance is given by the superposition of exponentials $X_h(\xi) = \exp(-2\lambda_h\xi)$ weighted by the coefficients C_h^2. From the standpoint of mixing performance, the variance at the outlet section, say at $\xi = \xi_L = 1/Pe$ should obviously be as low as possible. As the Pe number associated with microfluidic applications can take a wide range of values (order $Pe = 10^{-1}$ to 10^3) it follows that typical values of ξ_L range in the interval

$[10^{-3}, 10]$. From the expression of the variance equation (16), one gathers that, at high Pe values (e.g. $Pe = 10^3$), it is the entire eigenvalue spectrum, and not only the first (dominant) eigenvalue that determines the value of the scalar variance at the outlet section.

In the case of plug flow, the eigenfunction spectrum is simply given by $Y_h(y) = \cos(h\pi y)$, $h = 0, 1, \ldots$, where corresponding eigenvalues are given by $\lambda_h = \pi^2 h^2$. Next, we analyze the cases of shear and Poiseuille flows.

3.1. Shear flow

In this case, the dimensionless flow profile is given by $v_x(y) = 2y$, and the Sturm–Liouville problem reads as

$$Y''(y) + 2y\lambda Y(y) = 0. \tag{17}$$

By setting $z = \beta y$, $Y(y) = \eta(z)$, with $\beta = -(2\lambda)^{1/3}$, Eq. (17) transforms into

$$\eta''(z) - z\eta(z) = 0, \tag{18}$$

(where $\eta'(z) = \mathrm{d}\eta(z)/\mathrm{d}z$), equipped with the boundary conditions $\eta'(0) = \eta'(\beta) = 0$, for which the fundamental solution is a linear combination of the Airy functions $\mathrm{Ai}(z)$, $\mathrm{Bi}(z)$, $\eta(z) = C_1\mathrm{Ai}(z) + C_2\mathrm{Bi}(z)$ (see, e.g. [21]).

By imposing the first boundary condition, $\eta'(0) = 0$, one obtains $C_1 = \sqrt{3}C_2$. By enforcing the second boundary condition, $\eta'(\beta) = 0$, one obtains that the parameter β satisfies the equation:

$$\sqrt{3}\mathrm{Ai}'(\beta) + \mathrm{Bi}'(\beta) = 0. \tag{19}$$

The zeros of Eq. (19) form a non-positive sequence $\{\beta_h\}$, $h = 0, 1, \ldots$, diverging to $-\infty$. Therefore, the solution of the original problem in terms of ϕ is given by

$$\phi(x, y) = \sum_{h=0}^{\infty} C_h \, \mathrm{e}^{-2|\beta_h|^3 x/Pe} \left(\sqrt{3}\mathrm{Ai}(\beta_h y) + \mathrm{Bi}(\beta_h y)\right). \tag{20}$$

3.2. Poiseuille and generic flow profiles

In the case of the (dimensionless) Poiseuille flow, $v_x(y) = 6y(1 - y)$, or of a generic profile, no simple change of variables can be found to obtain an analytical solution. However, the Sturm–Liouville problem can be approached numerically, and the eigenvalue–eigenfunction spectrum can be computed by solving a system of two ordinary differential equations:

$$Z_1' = Z_2, \qquad Z_2' = -\lambda v_x(y) Z_1, \tag{21}$$

where $Z_1 = Y(y)$, and $Z_2 = Y'(y)$, with the initial condition $Z_1(0) = C$, $Z_2(0) = 0$, $C \neq 0$ being and arbitrary constant (e.g. unity). Specifically, the eigenvalues $\{\lambda_h\}$ are obtained by classical shooting method, as those values that yield $Z_2(1) = 0$.

The integration step-size was fixed by using the shear flow as a test case, by comparing numerical integration results with the analytical solution. The numerical integration was obtained by using a fourth-order Runge-Kutta routine, for which a step size Δy of order 10^{-5} was necessary to obtain a spectrum of $N_e = 300$ eigenvalues–eigenfunctions practically indistinguishable from that obtained analytically.

In the case of the Poiseuille flow, the use of this integration step size yielded a maximum error $|Y_h'(1)| \sim 10^{-3}$ for the highest modes. The corresponding eigenfunctions $Y_h(y)$ were sampled and recorded on 5×10^3 points equally spaced on the interval $[0, 1]$.

3.3. Results

Let us first analyze the validity of the Sturm–Liouville approximation. The Sturm–Liouville approach is rigorously valid only in the limit $1/\alpha \to \infty$, and therefore it is important to compare the solution stemming from this approach with that associated with the full boundary value problem. Fig. 9 shows the results of this comparison for a value $1/\alpha = 50$, which is no uncommon in micromixers (see, e.g. the example of the "Tee configuration mixer" reported in [2]). As it can be observed, for both Poiseuille and shear flow, no significant qualitative and quantitative discrepancies between the results of the two approaches can be appreciated, and this confirms the validity

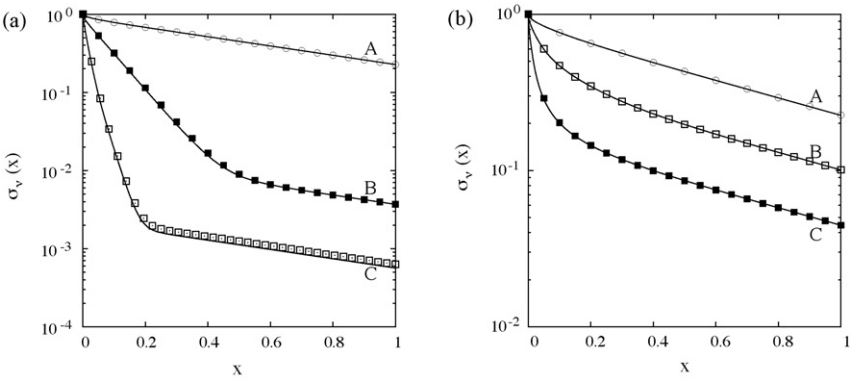

Fig. 9. Comparison between the solution of the full boundary value problem with the Sturm–Liouville approximation at $1/\alpha = 50$ and $Pe = 10$. The continuous lines represent the solution stemming from the Sturm–Liouville approach, the symbols the results of the finite volume solution of the full problem. Panel (a): Poiseuille flow. Panel (b): shear flow. Curve A and (◯) symbols: $n_s = 2$; curve B and (□) symbols: $n_s = 4$; curve C and (■) symbols: $n_s = 8$.

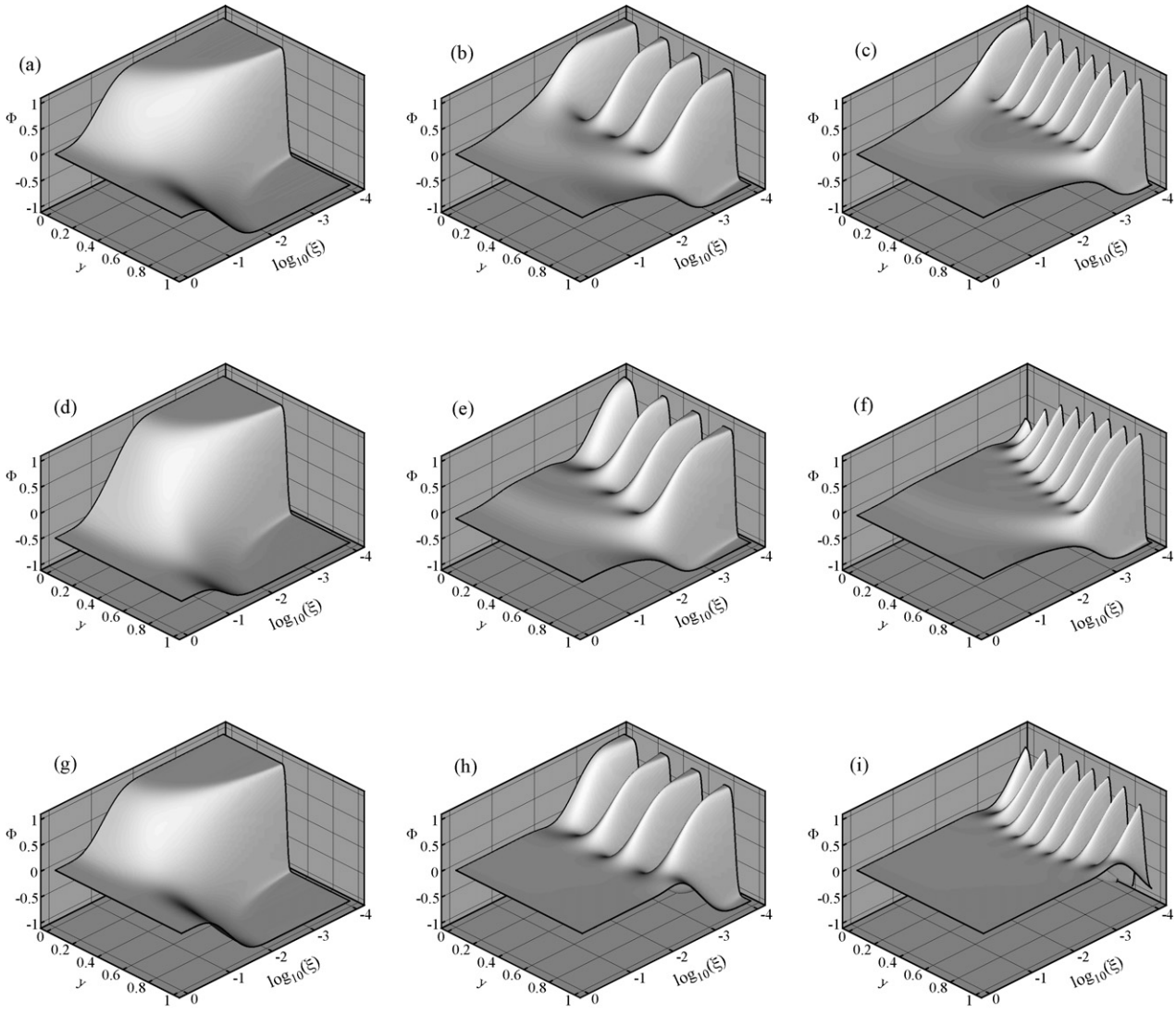

Fig. 10. Steady-state scalar concentration profiles $\Phi(\xi, y)$ for different degrees of lamination of the feed stream, and for different flow profiles. (a)–(c) Plug flow with $n_s = 2,\ 8,\ 16$, respectively; (d)–(f) shear flow with $n_s = 2,\ 8,\ 16$, respectively; (g)–(i) Poiseuille flow with $n_s = 2,\ 8,\ 16$, respectively.

of the Sturm–Liouville approach for $1/\alpha \geq 50$. Henceforth, we consider exclusively the Sturm–Liouville solution.

Let us compare the steady-state profiles associated with different degrees of lamination of the inlet stream in the three prototypical velocity profiles. Fig. 10 shows the homogenization profiles, $\Phi(\xi, y)$ for $n_s = 2, 8, 16$, as a function of the spanwise coordinate y and of the rescaled streamwise coordinate $\xi = x/Pe$ (note that the ξ-scale is logarithmic). These graphs can be interpreted in two different ways. At fixed Pe number, say $Pe = \overline{Pe}$, the value $\Phi(\xi, y)$, for $\xi \in [0, 1/\overline{Pe}]$, yields the scalar concentration value along the channel axis, from $x = 0$ to 1. On the other hand, by interpreting the scaled ξ coordinate as the reciprocal of the Pe number, $\xi = 1/Pe$, the profile $\Phi(\xi, y)$ at fixed ξ can be thought of as the outlet profile ($x = 1$) at the assigned $Pe = 1/\xi$ value.

In the case of a two-lamina feed, $n_s = 2$, mixing performances are similar in the three cases (Fig. 10 panels (a), (d) and (g)), i.e. for a low degree of lamination ($n_s = 2$ can be taken as representative of T-junction micromixers), homogenization is weakly affected by the flow profile, the best performance being that associated with the Poiseuille flow. Note that in the case of the shear flow the average scalar value attained at the outlet section is negative since the velocity is higher where the inlet profile is negative. As the degree of lamination increases from $n_s = 2$ up to 8, the impact of flow profile on mixing becomes evident (Fig. 10 panels (b), (e) and (h)). In this case, the performances of plug and shear flow are comparable, with a nearly homogeneous profile reached at $\xi > 0.1$ (i.e. $\log_{10}(\xi) > -1$), whereas, for the Poiseuille flow, a substantially flat profile is reached at $\xi > 10^{-3}$. These differences are amplified when the highest value of n_s is considered (Fig. 10 panels (c), (f) and (i)). For the case of shear flow (Fig. 10 panel (f)), an asymmetric profile is obtained as a consequence of the asymmetry of the velocity field, with a higher degree of mixing reached sooner near the static wall $y = 0$, since the low values of the local velocity implies higher contact times.

A more concise outlook at mixing homogenization can be gained by considering the scalar variance as an overall index

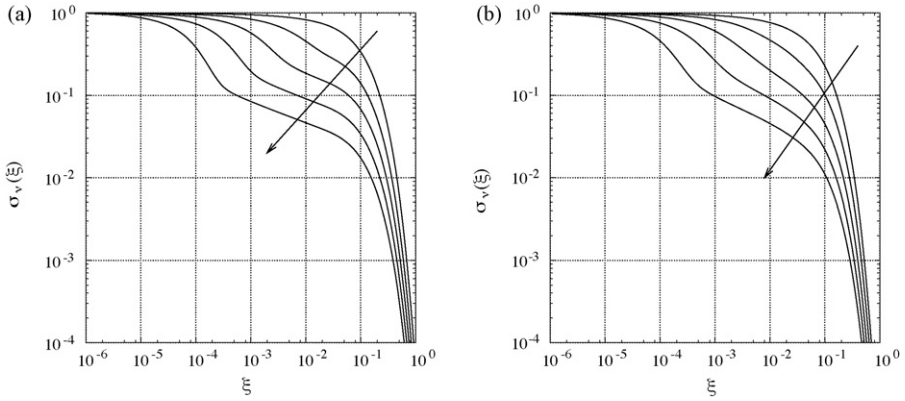

Fig. 11. Normalized scalar variance $\sigma_v(\xi)$ vs. the scaled axial coordinate, $\xi = x/Pe$, for (a) plug flow and (b): shear flow. The arrow indicates increasing degree of lamination of the inlet condition, $n_s = 2, 4, 8, 16, 32$.

of mixedness. Fig. 11 shows the decay of the normalized scalar variance $\sigma_v(\xi)$ versus the scaled coordinate $\xi = x/Pe$.

When interpreting the scaled ξ coordinate as the reciprocal of the Pe number, the curves depicted in Fig. 11 yield the correspondence between a prescribed value of the normalized scalar variance, say $\overline{\sigma}_v$, at the outlet section, and the corresponding value $\overline{\xi}$ that provides the assigned value of the normalized variance $\overline{\sigma}_v$. From the value $\overline{\xi}$, the channel length can be computed. For instance, assume the channel width, δ, the characteristic velocity U, and the bare molecular diffusivity $\mathcal{D}$, are held fixed, and suppose that a prescribed normalized variance, say $\sigma_v = 0.05$, is sought. Henceforth we refer to a degree of mixedness $\sigma_v = \mu$ as "$(1-\mu)\,100\%$ mixing", the present case corresponding to "95% mixing". For each degree of lamination n_s, the corresponding value ξ_{95} can be determined from the data depicted in Fig. 11. Since $\xi_{95} = 1/Pe = \mathcal{D}L/(\delta^2 U)$, it follows that the length required to accomplish this degree of mixedness is equal to $L_{95} = \xi_{95}\delta^2 U/\mathcal{D}$.

The behavior associated with plug and shear flows depicted in Fig. 11(a) and (b) shows that when a high mixing performance is required (e.g. 99% mixing), the degree of lamination impacts very little on the mixer length. The situation changes significantly when less strict performance is required. For instance, in the case of plug flow, the difference between the ξ_{99} values associated with $n_s = 2$ and 32 is of three orders of magnitude.

The overall mixing profiles associated with the Poiseuille flow (Fig. 12) show a behavior that is qualitatively and quantitatively different with respect to the two cases discussed above. First, even at high mixing performance, the associated ξ values depend significantly on the degree of lamination. Furthermore, when high degrees of lamination are considered (e.g. $n_s \geq 8$), mixing performances can improve by more than two orders of magnitude with respect to the corresponding case associated with plug or shear flows, whereas no significant improvement is observed at $n_s = 2$.

Since the velocity profile $v_x(y)$ directly enters the definition of the Sturm–Liouville eigenvalue problem (see Eq. (10)), it is reasonable to expect that a sensitive difference between mixing performances for the same inlet condition in different flow profiles should reflect into the eigenvalue–eigenfunction spectra of the corresponding Sturm–Liouville problems. However, the structure of the eigenvalues and eigenfunctions show that such differences do not justify neither the differences in the degree of mixedness observed for the three flow structures considered nor the striking performance of the Poiseuille flow.

Fig. 13 shows the first 10 eigenvalues (beside $\lambda_0 = 0$) for the different velocity profiles (panel (a)) and the first 3 eigenfunctions (beside $Y_0(y) = 1$) associated with the Poiseuille flow (panel (b)), compared with the corresponding eigenfunctions of the plug flow. As can be observed, neither the eigenvalue spectrum nor the eigenfunction structure display remarkable differences (compare, e.g. the eigenfunctions of Poiseuille and plug flows in Fig. 13(b)).

Therefore, from the functional form of $\phi(x, y)$ reported in Eq. (14) it follows that the improved mixing performances characterizing the Poiseuille flow can be attributed solely to the occurrence of significantly different spectra of projection coefficients $\{C_h\}$ with respect to the plug or shear flow. Fig. 14 shows the absolute value of the first coefficients C_h associated with the plug and Poiseuille flows, for two different inlet conditions, $n_s = 2$ and 8. In the first case (i.e. $n_s = 2$), the C_h-spectra (which can be referred to as the energy spectrum associated with the

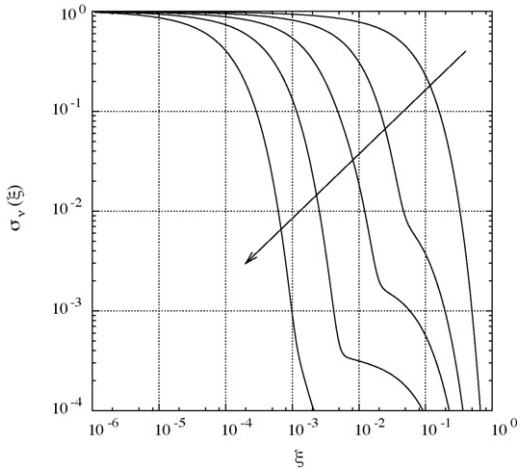

Fig. 12. Normalized scalar variance $\sigma_v^2(\xi)$ vs. the scaled axial coordinate, $\xi = x/Pe$, for the Poiseuille flow. The arrow indicates increasing degree of lamination of the inlet condition, $n_s = 2, 4, 8, 16, 32$.

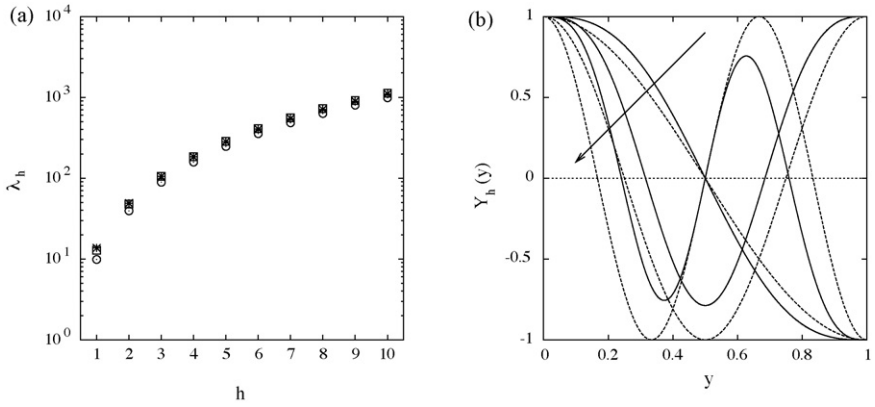

Fig. 13. Panel (a) first 10 eigenvalues of the Sturm–Liouville problem associated with plug (◯), shear (□), and Poiseuille flow (∗). Panel (b) comparison of the first three eigenfunctions for the Poiseuille (continuous lines) and the eigenfunctions $Y_h(y) = \cos(h\pi y)$ of the plug flow (dashed lines). The arrow indicates increasing order h = 1–3.

inlet condition) are quantitatively and qualitatively similar (note that the even-order coefficients vanish due to the symmetries of the flow profiles and of the inlet condition). The energy content associated with each eigenmode is monotonically decreasing in both cases. For a higher degree of lamination ($n_s = 8$), the distribution of energies among the eigenmodes shows significant differences. In the plug flow case, even though the higher energy content is concentrated onto the seventh mode, the first two odd coefficients are still significantly different from zero. Since they are associated to the slowest decaying eigenfunctions, they are bound to dominate the overall rate of decay, at moderate and high ξ values. In the case of the Poiseuille flow, these coefficients are essentially zero, and therefore the slowest decaying mode is that associated with the fifth eigenvalue. This explains why mixing performance is so different in these two cases.

It can be noted that the different values attained by the first two odd coefficients for the plug and Poiseuille flows is not a direct consequence of the eigenfunction structure (for instance, the first eigenfunction is quantitatively similar in the two cases, see Fig. 13(b)), but rather it is related directly to the fact that the scalar product that defines the coefficient value is weighted by the flow profile. To give an illustration of this point, let us consider the function:

$$\gamma_1(y) = \int_0^1 v_x(y)\,\phi_i^{(n_s)}(y)\,Y_1(y)\,\mathrm{d}y, \tag{22}$$

whose integral over the channel height yields the first coefficient C_1. Let us also define $\Gamma_1(y) = \int_0^y \gamma_1(y')\,\mathrm{d}y'$ (i.e. $C_1 = \Gamma_1(1)$). Fig. 15 shows the behavior of the functions γ_1 and Γ_1 for an inlet profile with $n_s = 8$ in the case of the plug and Poiseuille flows. As can be observed, the values of γ_1 are similar in most of the channel section with the exception of the regions near the wall, where, in the case of the Poiseuille flow, the behavior of γ_1 is dominated by the vanishing velocity profile $v_x(y)$ at the walls. As a consequence of the different behavior in these regions, the integral Γ_1 is positive in the case of the plug flow, whereas it oscillates about zero mean in the case of the Poiseuille flow (Fig. 15). Therefore, the major role played by

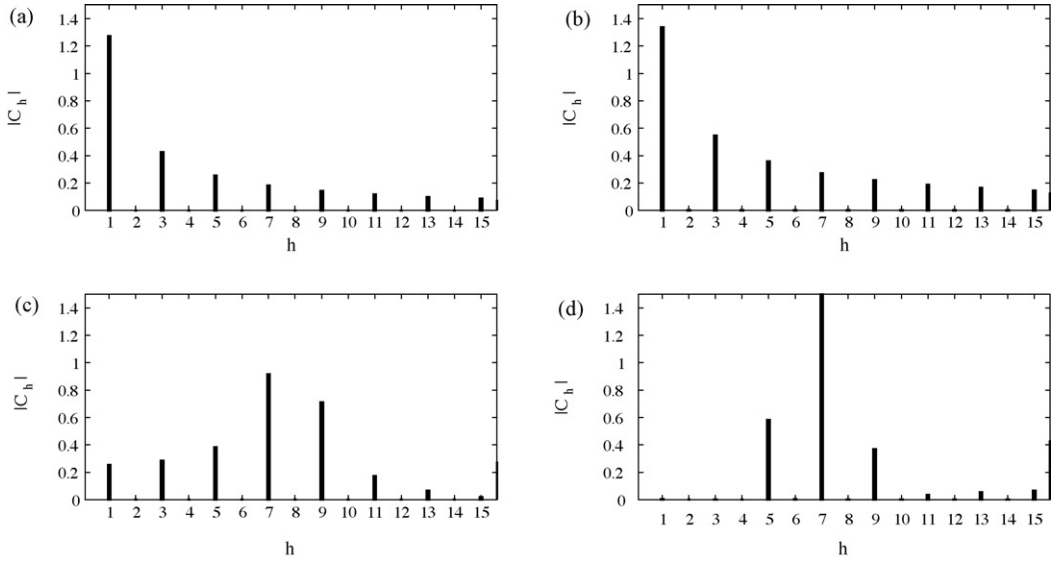

Fig. 14. Absolute value of expansion coefficients C_h of the steady-state scalar field in terms of the eigenfunctions of the Sturm–Liouville problem for (a) plug flow, $n_s = 2$; (b) Poiseuille flow, $n_s = 2$; (c) plug flow, $n_s = 8$; (d) Poiseuille flow, $n_s = 8$.

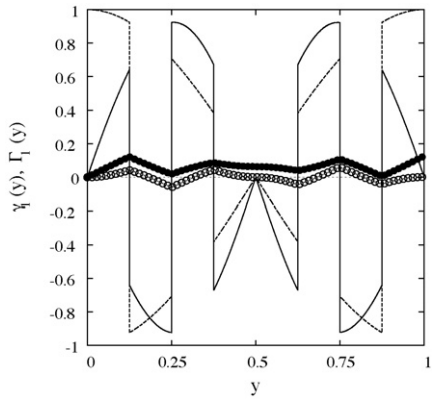

Fig. 15. Behavior of the functions $\gamma_1(y)$ and $\Gamma_1(y)$. Dashed line: γ_1—plug flow. Continuous line: γ_1—Poiseuille flow. (◯) Γ_1—plug flow. (◯) Γ_1—Poiseuille flow.

the flow profile in defining the spatial rate of homogenization of the advecting–diffusing scalar manifests itself through the weighted averages that define the projection coefficients C_h onto the Sturm–Liouville eigenbasis.

3.4. Dependence of mixing time and mixing length on lamellar thickness

As briefly discussed in the introductory section, for the case of plug flow, Eq. (8) can be also thought of as a one-dimensional unsteady diffusion problem, with the x coordinate playing the role of the (dimensionless) time-coordinate, and with the inlet condition $\phi^{(n_s)}(y)$ playing the role of the initial condition. A similar interpretation holds even in the case of non-constant flow profiles, as long as a variable effective diffusivity $D(y) = \mathcal{D}/v_x(y)$ is allowed. In this respect, the observations discussed above about the mixing length (i.e. the length necessary to achieve a prescribed degree of mixedness) can be also interpreted in terms of mixing time, where the relevant time scale is given by $\theta = L/U$ (i.e. time is made dimensionless with respect to the convective time scale). Then, the value ξ_μ to achieve a given level of mixedness $\sigma_v(1) = 1 - \mu/100$ can also be interpreted as proportional to the mixing time θ.

An important issue is to establish how, for a given degree of mixedness μ, the dimensionless mixing length ξ_s (or the dimensionless mixing time, for that matter) depends on the dimensionless lamellar thickness $s = 1/n_s$ [1,8]. Fig. 16(a) shows such dependence for the flow profiles considered in this article. For a comparison, panel (b) in the same figure reports the prediction ξ_s versus s obtained in the case of the plug flow equipped with periodic boundary conditions as discussed in [2], which represents the state of the art in the design of interdigital micromixers.

As can be observed, only the Poiseuille flow (lines E and F in Fig. 16(a)) verifies approximately the simple scaling $L \sim s^2$, independently of the prescribed degree of mixedness μ. The comparison with the case of plug flow equipped with periodic boundary conditions in the spanwise coordinate (lines A and B of Fig. 16(b)) shows that not only the power-law scaling, but even the order of magnitude of the ξ values is in good agreement. However, this agreement should be considered purely coincidental in that both the flow profile and the boundary conditions are different in the two cases.

In the case of plug (lines A and C) and shear flows (lines B and D), a substantially similar trend can be observed, namely, that the relationship between mixing length and lamellar thickness is strongly influenced by the degree of homogenization that is required. At a high degree of homogenization ($\mu = 0.01$, i.e. "99% mixing"—lines A and B), the mixing length scales very slowly with s. Also, note that the consideration of different boundary conditions with respect to the periodic case for the same plug flow profile (compare lines A and C of Fig. 16(a) with lines A and B of Fig. 16(b)) changes both the scaling relation and the order of magnitude of the predicted mixing length. An interesting phenomenon that is worth noting is the crossing of the ξ_{95} curves associated with plug and shear flow, which shows that, at low values of s, the performances of plug flow is better than that associated with shear flow, whereas the opposite occurs at high s values. This behavior can be put into correspondence with the spectral structure of the associated Sturm–Liouville and depends on the energy content of the expansion coefficients of the inlet profile with respect to the basis defined by the Sturm–Liouville operator. Specifically, the "95%" condi-

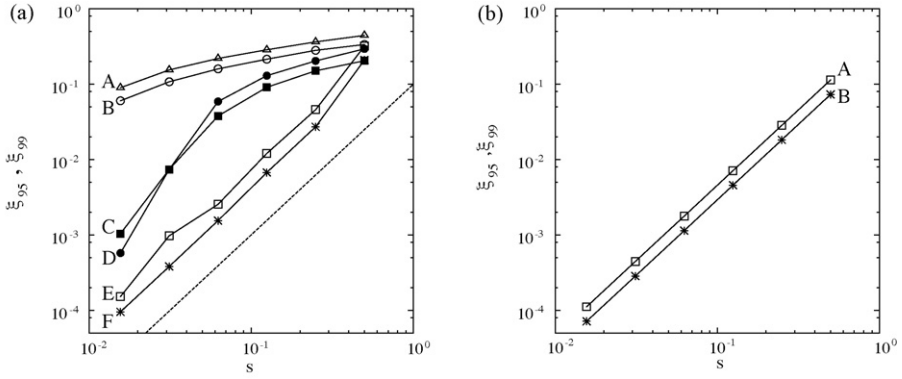

Fig. 16. Dimensionless length to achieve a prescribed degree of mixedness as a function of the dimensionless lamellar thickness $s = 1/n_s$. Panel (a) $n_s = 2, 4, 8, 16, 32, 64$. (+ and curve F), (■ and curve C), and (◯ and curve D) represent ξ_{95} for the Poiseuille, shear, and plug flows, respectively. (□ and curve E), (◯ and curve B), and (△ and curve A) represent ξ_{99} in the same order. The continuous line is the scaling $\xi = s^2$. Panel (b) plug flow with periodic boundary conditions; (+ and curve B) ξ_{95}; (□ and curve A) ξ_{99}.

tion is still relatively unmixed, so that several Sturm–Liouville modes are still active, and therefore the mixing performances still depend on the superposition of the active modes coefficients with respect to the decaying eigenmodes, which are ultimately dependent on the degree of lamination of the inlet scalar profile. In the case of the "99 %" curve, the level of mixedness is instead governed essentially by the dominant eigenvalue–eigenfunction, and therefore the shear flow performs better in that it possesses a higher dominant eigenvalue (faster decaying mode) with respect to the plug flow (see Fig. 13).

The data depicted in Fig. 16(a) can be considered as a design diagram for estimating the mixing length (or the mixing time) associated with a given flow profile. In this respect, it is worth observing that similar diagrams could be constructed with very modest computational effort for any type of parallel flow by solving the corresponding one-dimensional Sturm–Liouville problem, for which the shooting method discussed in this article provides a computationally simple strategy for obtaining the spectrum of eigenvalues/eigenfunctions.

3.5. Mixing in open and closed flows.

The equivalence between transient mixing in a closed system (with spatially dependent effective diffusivity) and axial mixing in an open system operating at steady state, discussed at the beginning of Section 3.4, poses the problem of establishing to what extent the knowledge achieved in the understanding of mixing processes in closed bounded flows can be straightforwardly extended to stationary inflow–outflow systems where streamwise diffusion can be neglected. In general terms, quantifying mixing in a closed (impermeable) system by the action of a stationary or time-periodic incompressible flow consists of determining the spectrum of eigenvalues–eigenfunctions associated with the advection–diffusion operator, in the case of an autonomous flow, or with the Poincaré operator associated with the non-autonomous advection–diffusion equation, in the case where the flow is time-periodic (see, e.g. [15]). For steady flows, the real part of the dominant (non-zero) eigenvalue of the advection–diffusion operator, say Λ_1, provides the slowest homogenization exponent Λ_{hom}, (i.e. $\Lambda_{\mathrm{hom}} = \Lambda_1$), that quantifies the exponential relaxation towards the equilibrium state, which is given by a constant scalar concentration field. In the case of time-periodic flows, the homogenization exponent Λ_{hom} is a function of the dominant eigenvalue (different from 1), say μ_1, of the Poincaré operator associated with the time-periodic advection–diffusion equation, and is given by $\Lambda_{\mathrm{hom}} = -\log|\mu_1|/T_{\mathrm{p}}$, where $|\mu_1| < 1$ and T_{p} is the flow period. For details, see e.g. [15,19,20]. The central issue in closed bounded systems is therefore to establish how, for a given convective flow, the dominant eigenvalue depends on the Pe parameter. In general, a scaling relation of the type $\Lambda_{\mathrm{hom}} \sim Pe^{-\beta}$ holds true (referred to as convection-enhanced mixing regime whenever $\beta < 1$), where the exponent β depends on the properties of the flow field and on its interaction with diffusion. Therefore, in the case of closed bounded flows the impact of the advecting flow on the mixing process manifests itself in defining the scaling of the eigenvalue spectrum of the advection–diffusion operator with the Pe number.

Under this respect, the case study discussed in this article, namely a generic parallel flow, is yet too simple to display a convection-enhanced regime for axial mixing. This is evident from the Pe-free formulation of the Sturm–Liouville problem expressed by Eq. (9). In point of fact, the independence of the eigenvalue spectrum $\{\lambda_h\}$ of Pe implies that the eigenvalues associated with the nonscaled coordinate x of the original problem, say $\tilde{\Lambda}_k$, are simply given by λ_k/Pe, i.e. the eigenvalues associated with the original problem depend on Pe as $\tilde{\Lambda}_k \sim 1/Pe$. Therefore, while the λ_ks depend on the specific flow profile, the exponent β that expresses the dependence of the eigenvalues of the original problem on Pe does not, and results always equal to unity. In this precise meaning, we claim that there cannot be any convection-enhanced diffusion phenomenon associated with steady-state axial mixing in a parallel flow (note that the same observation applies to a parallel flow in a three-dimensional channel, as long as the velocity components onto the cross-section are everywhere zero).

However, as showed throughout the article, this does not imply by all means that all of the velocity profiles yield the same mixing performance. In fact, the different performance does not manifest itself in terms of dominant decay exponent, but rather in defining what is the energy content of a prescribed inlet stream (i.e. the magnitude of the expansion coefficient) associated with each decaying mode.

4. Concluding remarks

We analyzed the impact of lamination degree (i.e. number and thickness of lamellae of the feed stream) on the advection–diffusion process taking place in a rectangular channel in the presence of plug, shear, and Poiseuille flows. In dimensionless form, the full advection–diffusion problem depends on two parameters, namely the Peclet number, Pe, and the channel aspect ratio, $1/\alpha$. At high values of $1/\alpha$ ($\alpha \to 0$), the steady-state solution is expected to become independent of α. Finite volume simulations suggest that this regime is reached for values of α that can depend significantly on the flow profile and on the degree of lamination.

In the limit of high-aspect ratio, the advection–diffusion process can be approached analytically by solving a Sturm–Liouville generalized diffusion problem in the spanwise coordinate, characterized by a variable (effective) diffusivity given by $1/(v_x(y)Pe)$. Besides the simple case of plug flow, an analytical solution of the Sturm–Liouville problem has been also derived for the shear flow in terms of Airy functions. For the Poiseuille flow and more generally for an arbitrary parallel flow, the Sturm–Liouville eigenvalue–eigenfunction spectrum problem can be approached by shooting algorithms. From the standpoint of computational cost, the advantage of using the Sturm–Liouville approach appears evident as soon as one considers that, at assigned flow profile, only a single computation of the eigenvalue–eigenfunction spectrum is necessary, independently of the Pe number, whereas the solution of the full boundary value transport problem requires to run

a simulation for each assigned *Pe*. Once the Sturm–Liouville spectrum has been computed, one is left with the determination of the projection coefficients, which requires simple quadratures. Beyond computational time requirements, the advantage of using the Sturm–Liouville approach can be appreciated also in terms of memory requirements in that it allows to recast a two-dimensional problem into a one-dimensional eigenvalue problem.

The analysis of the Sturm–Liouville solution shows that almost independently of the degree of lamination, plug and shear flows perform similarly in terms of mixing efficiency, quantified by the velocity-weighted scalar variance. In the case of the Poiseuille flow, instead, mixing efficiency can be enhanced by orders of magnitude for high degrees of lamination. On the other hand, at $n_s = 2$, that is, in the case of a T-junction mixer, the enhancement is barely appreciable.

From the design standpoint, an important issue is to establish how the mixer length depends upon the lamination thickness. Simple estimates, based on the diffusive timescale in a spatially periodic array of alternating lamellae, forecast a scaling $L \sim s^2$ of the mixer length L necessary to obtain an assigned level of mixedness, and the characteristic size s of the lamination thickness. We found that, in general, this scaling is hardly verified. For instance in the case of plug and shear flows, the relationship between L and s depends upon the degree of mixedness required. However, the scaling relation is not represented by a power law. The $L \sim s^2$ is instead found where less expected, i.e. in the case of Poiseuille flow. This behavior can be put into correspondence with the peculiar spectral structure that highly laminated feed streams possess with respect to the eigenbasis stemming from Sturm–Liouville generalized diffusion problem.

The approach outlined is this article can be considered an extension of the widely used analytical estimate of mixing length/time in interdigital micromixers obtained by recasting the steady-state advection–diffusion problem into a one-dimensional pure diffusion equation equipped with periodic boundary conditions. We showed that these approximations can lead to a significant overestimation of mixing efficiency. The spectral representation of the solution provides a direct insight on the impact of the flow profile on mixing efficiency, and can in principle be used for designing flow profiles (e.g. by combining an overall pressure drop with electroosmosis) that minimize the projection coefficients of the inlet profile onto the slowest decaying modes.

Appendix A

In this appendix, we derive the $L \sim s^2$ scaling that is widely used in the literature for estimating the dimensions and the operating conditions of micromixers (see, e.g. [1] and therein cite references). With the simplifying assumptions of uniform flow, periodic boundary conditions and high-aspect ratio $\alpha \to 0$, the (dimensional) steady-state advection–diffusion equation reads as

$$U\frac{\partial\hat{\phi}}{\partial x} = \mathcal{D}\left(\frac{\partial^2\hat{\phi}}{\partial x^2} + \frac{\partial^2\hat{\phi}}{\partial y^2}\right), \tag{23}$$

where $0 \le x \le L$ and $0 \le y \le \delta$ are the streamwise and spanwise coordinates, and U is the characteristic (mean) velocity (see Fig. 1).

The analytical solution of this simplified problem setting can be expressed in terms of Fourier series $\hat{\phi}(x, y) = \sum_{h=1}^{\infty} C_h X_h(x) \sin(2h\pi y/\delta)$, where $X_h(x) = \exp(-\Lambda_h x)$, $\Lambda_h = 4\pi^2 h^2 \mathcal{D}/(\delta^2 U)$. For an assigned degree of lamination n_s of the feed stream (see. Eq. (4)), the coefficients $C_h^{(n_s)}$ (we use here the superscript "(n_s)" to indicate that the Fourier coefficients refer to an inlet profile $\phi_i^{(n_s)}(y)$ given by Eq. (4)) are characterized by an invariant energy spectrum. Specifically, only the coefficients $\{C_j^{(n_s)}\}$ with $j = n_s/2 + i\,n_s$ $(i = 0, 1, 2, \ldots)$ are different from zero. Furthermore, when two different degrees of lamination, say $n_s = n_1$ and $n_s = n_2$ are considered, then it results that $C_{n_1/2+i\,n_1}^{(n_1)} = C_{n_2/2+i\,n_2}^{(n_1)}$ for any integer i (see Fig. A1).

Next, assume that a given level of mixedness of the scalar variance at the outlet section, say $\overline{\sigma}$, is fixed. For values of L larger than $\delta^2 U/(4\pi^2\mathcal{D})$, the leading term in the Fourier series is associated with the first nonvanishing coefficient which is $C_{n_s/2}$. Therefore $\overline{\sigma} \sim |C_{n_s/2}^2| \exp(-4\pi^2(n_s/2)^2\mathcal{D}L/(\delta^2 U))$. When this relationship is made explicit with respect to L, one obtains

$$L \approx \frac{\delta^2 U|\log(\overline{\sigma}/|C_{n_s/2}|)|}{\pi^2\mathcal{D}n_s^2}. \tag{24}$$

Eq. (24) implies a scaling relation $L \sim s^2$ between the mixing length and the lamellar thickness $s = \delta/n_s$. It is also worth noting that the scaling relation just obtained (within the approximations stated above) is independent of the level of mixedness $\overline{\sigma}$.

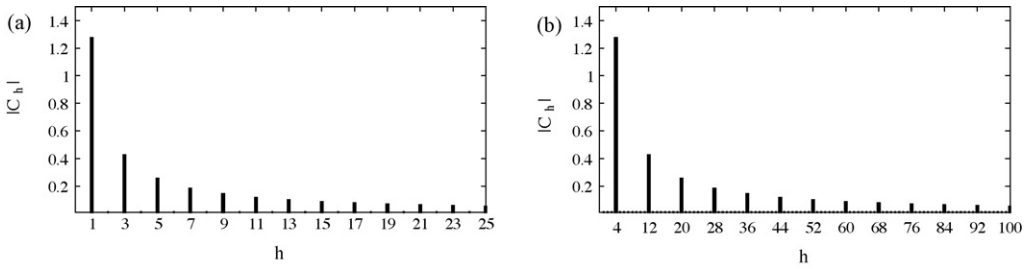

Fig. A1. Coefficient spectrum associated with different degrees of lamination, n_s, of the feed stream for the sine Fourier series representation of the solution of Eq. (23) equipped with periodic boundary conditions: (a) $n_s = 2$ and (b) $n_s = 8$.

References

[1] P. Tabeling, Introduction to Microfluidics, Oxford University Press, Oxford, 2005.

[2] W. Ehrfeld, V. Hessel, H. Löwe, Microreactors. New Technology for Modern Chemistry, Wiley–VCH, Weinheim, 2000.

[3] P. Lob, H. Pennemann, V. Hessel, Y. Men, Impact of fluid path geometry and operating parameters on l/l-dispersion in interdigital micromixers, Chem. Eng. Sci. 61 (2006) 2959–2967.

[4] A.E. Kamholz, B.H. Weigls, B.A. Finlayson, P. Yager, Quantitative analysis of molecular interaction in a microfluidic channel: the T-sensor, Anal. Chem. 71 (1999) 5340–5347.

[5] B.H. Weigl, P. Yager, Microfluidic diffusion-based separation and detection, Science 283 (1999) 346–347.

[6] C.N. Baroud, F. Okkels, L. Menetrier, P. Tabeling, Reaction–diffusion dynamics: confrontation between theory and experiment in a microfluidic reactor, Phys. Rev. E 67 (2003) 060104.

[7] V. Hessel, S. Hardt, F. Schönfeld, Laminar mixing in different interdigital micromixers. I. Experimental characterization, AIChE J. 49 (3) (2003) 566–577.

[8] S. Hardt, F. Schönfeld, Laminar mixing in different interdigital micromixers. II. Numerical simulations, AIChE J. 49 (3) (2003) 578–584.

[9] N. Aoki, S. Hasebe, K. Mae, Micromixing in microreactors: effectiveness of lamination segments as a form of feed on product distribution for multiple reactions, Chem. Eng. J. 101 (2004) 323–331.

[10] S. Hardt, H. Pennemann, F. Schönfeld, Theoretical and experimental characterization of a low-Reynolds number split-and-recombine mixer, Microfluid Nanofluid 2 (2006) 237–248.

[11] V. Hessel, H. Lowe, A. Muller, G. Kolb, Chemical Micro Process Engineering, Wiley–VCH, Weinheim, 2005.

[12] D. Li, Single phase electrokinetic flow in microchannels, in: S. Kandlikar, D. Garimells, S. Li, M. Colin (Eds.), Heat Transfer and Fluid Flow in Minichannels and Microchannels, Elsevier, 2005, pp. 137–173.

[13] G. Karniandakis, A. Beskok, N. Aluru, Microflows and Nanoflows, Springer-Verlag, New York, 2005.

[14] I.M. Sokolov, A. Blumen, Diffusion-controlled reactions in lamellar systems, Phys. Rev. A 43 (1991) 5698–5701.

[15] S. Cerbelli, V. Vitacolonna, A. Adrover, M. Giona, Eigenvalue–eigenfunction analysis of infinitely fast reactions and micromixing regimes in regular and chaotic bounded flows, Chem. Eng. Sci. 59 (2004) 2125.

[16] J.P. Gleeson, Infinitely fast reactions in micromixers, in: 2006 NSTI Nanotechnology Conference and Trade Show—NSTI Nanotech 2006 Technical Proceedings, vol. 2, 2006, pp. 509–512.

[17] R.B. Bird, W.E. Stewart, E.N. Lightfoot, Transport Phenomena, second ed., John Wiley & Sons, New York, 2002.

[18] T.M. Squires, S.R. Quake, Microfluidics: fluid physics at the nanoliter scale, Rev. Mod. Phys. 77 (2005) 977–1026.

[19] S. Cerbelli, A. Adrover, F. Creta, M. Giona, Foundations of laminar chaotic mixing and spectral theory of linear operators, Chem. Eng. Sci. 61 (2006) 2754–2761.

[20] M. Giona, A. Adrover, S. Cerbelli, V. Vitacolonna, Spectral properties and transport mechanisms of partially chaotic bounded flows in the presence of diffusion, Phys. Rev. Lett. 92 (2004) 114101.

[21] M. Abramowitz, I.A. Stegun, Handbook of Mathematical Functions with Formulas, Graphs, and Mathematical Tables, National Bureau of Standards Applied Mathematics Series, Washington, DC, 1964.